NUMERICAL SIMULATION OF MELTING AND CRYSTALLIZATION OF CdZnTe INDUCED BY PULSED LASERS

Robert Černý[1], Jan Toman[2], Petr Přikryl[3], Elena Gatskevich[4]

[1]Department of Structural Mechanics, Faculty of Civil Engineering, Czech Technical University, Thákurova 7, 166 29 Prague 6, Czech Republic
[2]Department of Physics, Faculty of Civil Engineering, Czech Technical University, Thákurova 7, 166 29 Prague 6, Czech Republic
[3]Mathematical Institute of the Academy of Sciences of the Czech Republic, Žitná 25, 115 67 Prague 1, Czech Republic
[4]Institute of Electronics, National Academy of Sciences of Belarus, 22 Logoiskii trakt, 220090 Minsk, Belarus
Email: cernyr@fsv.cvut.cz, toman@fsv.cvut.cz, prikryl@math.cas.cz, gatskevich@inel.bas-net.by

Abstract

A set of numerical simulations of pulsed laser-induced melting and crystallization of CdZnTe is done using a computational model of rapid phase transitions in binary semiconducting systems. The temperature and concentration fields, and the position and velocity of the phase interface are calculated as functions of the laser energy density for two types of lasers, namely Nd:YAG laser (16 ns FWHM pulse duration, 266, 355, 532 nm wavelengths) and ruby laser (80 ns FWHM, 694 nm). The results obtained for both the lasers are discussed and recommendations for optimization of experimental setups are given.

Key words: CdZnTe, pulsed laser, melting, solidification, numerical simulations

1 Introduction

The application of pulsed laser annealing and alloying to II-VI compounds and the ternary alloys based on them can be roughly divided into three directions: i) doping and implantation, ii) modification of structural, electrical and optical properties, iii) changes of composition. Some procedures are commonly used in the processing of semiconductors, as for example the recrystallization of an amorphized layer due to ion implantation or other kinds of structure modification. Similarly as for group IV elements or III-V compounds, samples processed by laser annealing show analogous or better electrical and optical parameters in comparison with thermal annealing [1]. However, the pulsed laser irradiation induces some morphological (cracks, spongy structures) [2] and chemical (lateral or depth redistribution of elements) changes [3], which strongly depend on the laser power, wavelength and number of pulses applied in a surface modification. For an industrial application, the origin of these changes has to be studied in a more detail as a function of laser irradiation parameters and of the way of the sample preparation (thin films, bulk material, substrate material).

In this paper, the effects induced by pulsed laser irradiation of CdZnTe pseudobi-

nary alloy are studied by means of numerical modeling. Two lasers with different wavelengths and different pulse durations are chosen to analyze the influence of laser irradiation parameters on the basic characteristics of the melting and solidification process.

2 Mathematical model

We will employ the model of nonequilibrium melting and solidification of II-VI binary alloys formulated by Přikryl, Segeth and Černý [4]. We consider a binary alloy consisting of components A, B that is irradiated by a laser pulse with the energy density $E = \int_0^\infty I_0(t)\mathrm{d}t$, where $I_0(t)$ is the power density of the pulse.

Supposing that the dimensions and symmetry of the sample allow us to treat it in one space dimension, the balance equations of internal energy of the system and the balance equations of mass of the component A in both the phases can be formulated as follows.

Internal energy:

$$\rho c_\mathrm{l}\frac{\partial T_\mathrm{l}}{\partial t} = \frac{\partial}{\partial x}\left(K_\mathrm{l}\frac{\partial T_\mathrm{l}}{\partial x}\right) + (1-R(t))\alpha_\mathrm{l}(x)I_0(t)\exp(-\int_0^x \alpha_\mathrm{l}(\eta)\mathrm{d}\eta),$$

$$x \in (0, Z(t)), \quad t > 0, \tag{1}$$

$$\rho c_\mathrm{s}\frac{\partial T_\mathrm{s}}{\partial t} = \frac{\partial}{\partial x}\left(K_\mathrm{s}\frac{\partial T_\mathrm{s}}{\partial x}\right) + (1-R(t))\alpha_\mathrm{s}(x)I_0(t)\times$$

$$\times \exp(-\int_0^{Z(t)} \alpha_\mathrm{l}(\eta)\mathrm{d}\eta - \int_{Z(t)}^x \alpha_\mathrm{s}(\eta)\mathrm{d}\eta), \quad x \in (Z(t), l), \quad t > 0, \tag{2}$$

where T is the temperature, ρ is the density, c the specific heat, K the thermal conductivity, $R(t)$ the reflectivity, $\alpha(x)$ the optical absorption coefficient, l is the thickness of the sample, and the subscripts l, s denote the liquid and the solid phase, respectively.

Mass of the component A:

$$\frac{\partial C_\mathrm{A,l}}{\partial t} = \frac{\partial}{\partial x}\left(D_\mathrm{l}\frac{\partial C_\mathrm{A,l}}{\partial x}\right), \quad x \in (0, Z(t)), \quad t > 0, \tag{3}$$

$$\frac{\partial C_\mathrm{A,s}}{\partial t} = \frac{\partial}{\partial x}\left(D_\mathrm{s}\frac{\partial C_\mathrm{A,s}}{\partial x}\right), \quad x \in (Z(t), l), \quad t > 0, \tag{4}$$

where D is the diffusion coefficient, C_A is the concentration of the component A which is defined as $C_\mathrm{A} = \rho_\mathrm{A}/\rho$, where ρ_A is the mass of the component A per unit volume of the mixture.

In formulating the corresponding balance equations at the solid/liquid interface $Z(t)$, we employ the theory of discontinuity surfaces and write

$$\rho L_\mathrm{m}\frac{\mathrm{d}Z}{\mathrm{d}t} = -K_\mathrm{l}\left(\frac{\partial T_\mathrm{l}}{\partial x}\right)_{x=Z(t)-} + K_\mathrm{s}\left(\frac{\partial T_\mathrm{s}}{\partial x}\right)_{x=Z(t)+}, \tag{5}$$

$$(C_\mathrm{A,l} - C_\mathrm{A,s})\frac{\mathrm{d}Z}{\mathrm{d}t} = -D_\mathrm{l}\left(\frac{\partial C_\mathrm{A,l}}{\partial x}\right)_{x=Z(t)-} + D_\mathrm{s}\left(\frac{\partial C_\mathrm{A,s}}{\partial x}\right)_{x=Z(t)+}, \tag{6}$$

where L_{m} is the latent heat of fusion.

Besides the balance conditions, two additional conditions at the solid/liquid interface have to be formulated, namely the liquidus and solidus curves of the phase diagram,

$$T_{\mathrm{l}} = T_m \left(C_{\mathrm{A,l}}, \frac{\mathrm{d}Z}{\mathrm{d}t} \right), \tag{7}$$

$$T_{\mathrm{s}} = T_c \left(C_{\mathrm{A,s}}, \frac{\mathrm{d}Z}{\mathrm{d}t} \right), \tag{8}$$

where T_m is the liquidus curve, and T_c is the solidus curve, and finally we introduce the Wilson-Frenkel interface response function

$$\frac{\mathrm{d}Z}{\mathrm{d}t} = f\nu \left[1 - \exp\left(-\frac{\Delta G}{k_B T_Z} \right) \right], \tag{9}$$

where

$$\Delta G = \Delta\mu_{\mathrm{A}} C_{\mathrm{A,l,Z}} + \Delta\mu_{\mathrm{B}} C_{\mathrm{B,l,Z}}, \tag{10}$$

T_Z, C_Z are the temperature and the concentration at the interface, resp., ΔG, $\Delta\mu$ are the changes of Gibbs energy and chemical potential, resp., due to the phase transition, and f, ν are frequency factors.

The practical implementation of the nonequilibrium phase diagram (7), (8) is performed using the nonequilibrium segregation coefficient k in our model, $k = C_{\mathrm{A,s}}/C_{\mathrm{A,l}}$. The relation of k to the equilibrium segregation coefficient k_o can be expressed for instance by the formula derived by Aziz [5]

$$k(T_Z) = k_o(T_Z) + [1 - k_o(T_Z)] \exp\left(\frac{D_i}{\lambda \frac{\mathrm{d}Z}{\mathrm{d}t}} \right), \tag{11}$$

where D_i is the diffusion coefficient through the phase interface, λ is the interatomic distance. The initial and boundary conditions are formulated in a common way (see e.g. [6]).

2 Computer implementation

In solving the problem (1)–(4), (5)–(9) with the appropriate initial and boundary conditions, we employ first the Landau transformation [7] to map both the liquid and the solid domain onto a fixed space interval $\xi \in [0, 1]$.

To solve the fixed-domain initial-boundary value problem obtained we employ the Galerkin finite element method. Supposing that the initial state $\{T\}_t$, $\{C_{\mathrm{A}}\}_t$ is known (for $t = 0$ it is given by the initial conditions), we get a system of nonlinear algebraic equations for $\{T\}_{t+\Delta t}$, $\{C_{\mathrm{A}}\}_{t+\Delta t}$ which can be schematically expressed in the form (see [4] for more details)

$$[\overline{H}_T]\{T\}_{t+\Delta t} = [\overline{P}_T]\{T\}_t + \{\overline{F}_T\} \tag{12}$$

$$[\overline{H}_C]\{C_{\mathrm{A}}\}_{t+\Delta t} = [\overline{P}_C]\{C_{\mathrm{A}}\}_t + \{\overline{F}_C\}. \tag{13}$$

To proceed with the solution from time t to time $t+\Delta t$ we have to solve the system of equations (12), (13) for the unknowns $\{T\}_{t+\Delta t}$, $\{C_{\mathrm{A}}\}_{t+\Delta t}$, and $\dot{Z}(t+\Delta t)$ as $Z(t+\Delta t)$ can be calculated from the value of interface velocity and $Z(t)$ in our algorithm.

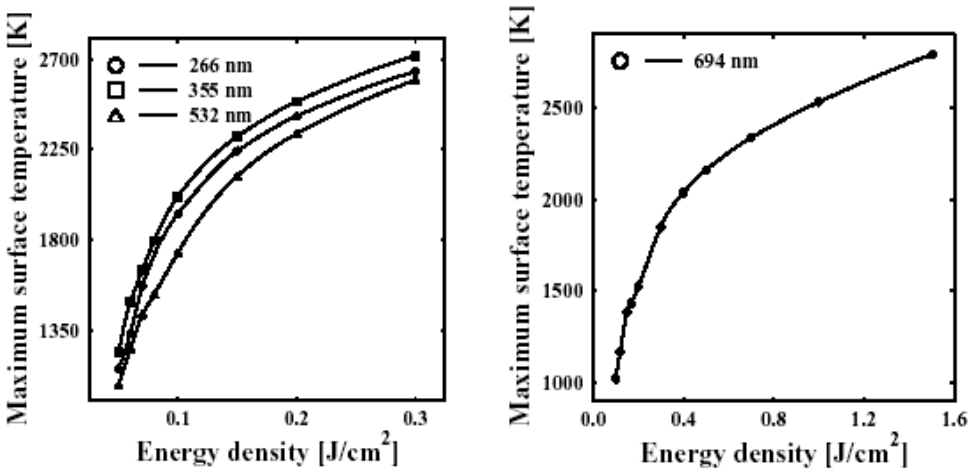

Fig. 1 Maximum surface temperature of CdZnTe as a function of the laser energy density a) Nd:YAG laser, b) ruby laser

The iteration algorithm used to solve the nonlinear problem under consideration is based on the successive approximation approach with underrelaxation. Its final purpose is to find the temperature and concentration fields in the sample and the position and velocity of the phase interface such that the interface response condition (9) is satisfied within accuracy δ in each time step.

3 Numerical simulations

In the numerical simulations, we modeled the melting and solidification of CdZnTe induced by Nd:YAG laser (16 ns FWHM, 266, 355, 532 nm) and ruby laser (80 ns FWHM, 694 nm). The initial content of zinc in the CdZnTe pseudo-binary was assumed to be 4% in all calculations. The energy density of the laser pulse varied from 0.01 Jcm^{-2} to 0.30 Jcm^{-2} for the Nd:YAG laser and from 0.1 Jcm^{-2} to 1.50 Jcm^{-2} for the ruby laser. The shape of the laser pulse $I_0(t)$ employed in the computations was obtained by experimental measurements. The thermodynamic parameters of CdZnTe were taken from [8], the optical parameters from [9].

The main outputs of the calculations were the temperature and concentration fields, and the positions and velocities of the phase interface. Examples of computational results are given in Figs. 1a,b and 2a,b.

Fig. 1a,b shows the maximum surface temperatures T_s for both Nd:YAG and ruby lasers as functions of laser energy density. The shapes of the $T_s(E)$ curves roughly correspond to a square root function, $T_s \sim \sqrt{E}$. They are very similar for both the lasers and all the wavelengths studied, the higher energy densities used for the ruby laser being necessary due to its longer pulse duration. This is a different behavior compared for instance with Si [10] where $T_s \sim E^2$. The main reason for this fact is probably an intensive evaporation of CdZnTe at higher temperatures accompanied by cooling of the surface due to the consumption of the latent heat of evaporation. The differences in the maximum surface temperatures for different wavelengths of Nd:YAG laser in Fig. 1a are due to the differences in the incident laser reflectivities and optical absorption coefficients. The

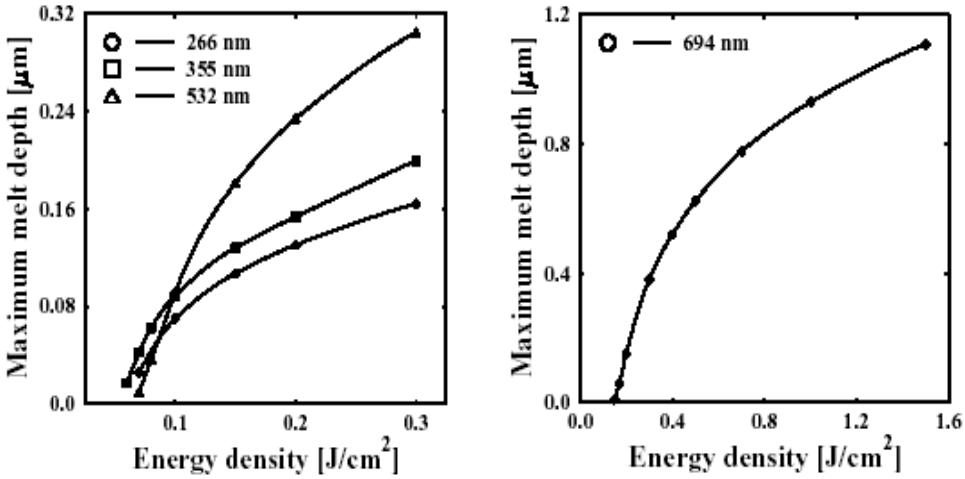

Fig. 2 Maximum melt depth of CdZnTe as a function of the laser energy density a) Nd:YAG laser, b) ruby laser

lowest reflectivity for both the solid and the liquid is at 532 nm, while the highest reflectivity is at 266 nm. However, the optical absorption coefficients are lowest at 532 nm, highest for 266 nm, and for 355 nm only slightly lower than for 266 nm. These effects are counteracting and for surface temperatures their combination has led to the highest values for 266 nm, lowest values for 532 nm.

Fig. 2a,b shows the maximum melt depths $d_{\max}$ as functions of laser energy density for both studied lasers. The shapes of all curves are very similar again, approximately $d_{\max} \sim \sqrt{E}$, which differs from those determined earlier for other materials (e.g. for Si, $d_{\max} \sim E^2$, see [10]). The reason is probably again the intensive evaporation which decreases the amount of absorbed laser energy that can be used for heating the underlying layers. The maximum melt depth for ruby laser and for comparable surface temperatures was several times higher than that for Nd:YAG laser. The reason is the longer pulse duration of ruby laser than that of Nd:YAG laser leading to more effective heat conduction deeper into the material, longer melt duration and logically also higher melt depth.

4 Conclusions

The basic characteristic parameters of pulsed laser-induced melting and crystallization of CdZnTe determined for two different lasers and four different wavelengths can be effectively employed by the experimentalists in the optimization of experimental setup. The melting thresholds (see Fig. 2a,b) show the lower limit of laser energy density that can be used in the experiments for CdZnTe surface modifications. The decision on higher energy density limit is more difficult. The main criterion for such decision is that the evaporation must not be too intensive because the quality of the surface would be low. Therefore, the energy density should not be too high. Fig. 2a,b show that the initial parts of the $d_{\max}(E)$ curves are for both the lasers and all wavelengths almost linear and later the curves begin to resume the final $\sim \sqrt{E}$ shape. These initial linear parts of the $d_{\max}(E)$ functions can be clearly distinguished so that there is a good reason for to conclude that evaporation does

not yet play any important role in the process. Therefore, the end of the linear parts can be taken as the higher limit of laser energy density. Taking the above analysis into account, we can conclude that the energy density "window" suitable for experiments is: for Nd:YAG laser from 0.07 Jcm^{-2} to 0.10 Jcm^{-2}, for ruby laser from 0.15 Jcm^{-2} to 0.30 Jcm^{-2}. The window for Nd:YAG laser is very narrow and problems with exact setting of laser energy density can be anticipated. Ruby laser is a safer solution from this point of view.

Acknowledgement

This paper is based upon work supported by the Grant Agency of the Czech Republic, under grants # 106/01/0648 and # 201/01/1200.

References

[1] Neumann-Spallart M., Levy-Clement C., Grabner, G., Fast Annealing of II-VI Compounds by Pulsed Laser Irradiation. *J. Phys D (UK)*, **27**, pp. 407-413, 1994.

[2] Zhao J.H., Li X.Y., Liu H., Jiang R.Q., Liu Z.P., Hu Z.H., Gong H.M., Fang J.X., Damage threshold of HgCdTe induced by continuous-wave CO_2 laser. *Appl. Phys. Lett*, **74**, pp. 1081-1083, 1999.

[3] Scepanovic M., Jevtic M., Raman studies of compositional changes in $Hg_{1-x}Cd_x$ Te due to pulsed laser annealing in air. *Solid State Phenomena*, **61/62**, pp. 251-255, 1998.

[4] Přikryl P., Segeth K., Černý R., Computational Modeling of Pulsed Laser-Induced Phase Change Processes in II-VI Semiconductors. Proceedings of Heat Transfer VII, B. Sunden, C.A. Brebbia (eds.), WIT Press, Southampton 2002, 205-214.

[5] Aziz, M.J., Model for solute redistribution during rapid solidification. *J. Appl. Phys.*, **53**, pp. 1158–1168, 1982.

[6] Černý, R., Přikryl, P., Computational model of nonequilibrium phase transitions in a Si-Ge system. *Computational Materials Science*, **10**, pp. 468–474, 1998.

[7] Landau, H., Heat conduction in a melting solid. *Quart. of Applied Math.*, **8**, pp. 81–94, 1950.

[8] Černý, R., Kalbáč, A., Přikryl, P., Computational modeling of CdZnTe crystal growth from the melt. *Computational Materials Science*, **17**, pp. 34–60, 2000.

[9] Kim, C.C., Daraselia, M., Garland, J.W., Sivananthan, S., Temperature dependence of the optical properties of CdTe. *Phys. Rev. B*, **56**, pp. 4786–4797, 1997.

[10] Černý, R., Šášik, R., Lukeš, I., Cháb, V., Excimer Laser Induced Melting and Solidification of Monocrystalline Si: Equilibrium and Nonequilibrium Models. *Phys. Rev. B*, **44**, pp. 4097-4102, 1991.